

Effect of Hydrodynamic Heterogeneity on Micromixing in a Taylor-Couette Flow Reactor with Lobed Inner Cylinder

Lu Liu¹, Xiaogang Yang¹, Jie Yang¹, Guang Li¹, and Yanqing Guo¹

¹University of Nottingham - Ningbo China

September 11, 2020

Abstract

Effect of hydrodynamic heterogeneity on micromixing intensification in a Taylor-Couette flow reactor (TC) with variable configurations of inner cylinder has been investigated by adoption of a parallel competing iodide-iodate reaction system. Two types of inner cylinder, circular inner cylinder and lobed inner cylinder (CTC and LTC), were used to generate hydrodynamic heterogeneity for comparison of the micromixing intensification, focusing on the effects of the Reynolds number of the TC reactor, the acid concentration, and the feeding time. The Segregation index (X_s) was employed to evaluate the micromixing efficiency. It was revealed that X_s decreases with the increase of Reynolds number and feeding time but increases with the increase of acid concentration for both the CTC and LTC. However, the LTC does present a better micromixing performance at various operating conditions than that of the CTC as affirmed by both the experimental and computational fluid dynamics (CFD) simulation results.

Abstract

Effect of hydrodynamic heterogeneity on micromixing intensification in a Taylor-Couette flow reactor (TC) with variable configurations of inner cylinder has been investigated by adoption of a parallel competing iodide-iodate reaction system. Two types of inner cylinder, circular inner cylinder and lobed inner cylinder (CTC and LTC), were used to generate hydrodynamic heterogeneity for comparison of the micromixing intensification, focusing on the effects of the Reynolds number of the TC reactor, the acid concentration, and the feeding time. The Segregation index (X_s) was employed to evaluate the micromixing efficiency. It was revealed that X_s decreases with the increase of Reynolds number and feeding time but increases with the increase of acid concentration for both the CTC and LTC. However, the LTC does present a better micromixing performance at various operating conditions than that of the CTC as affirmed by both the experimental and computational fluid dynamics (CFD) simulation results.

Keywords: Geometry modification; Micromixing efficiency; Segregation index; Micromixing time.

*Corresponding author: Tel: +86-574-88182419 E-mail: Xiaogang.Yang@nottingham.edu.cn

(XY)

Introduction

During the synthesis of various micro/nano particles, the hydrodynamics of the mixing in the reactors has been recognised as playing a determinant role in determining the synthesised particle properties. In particular, micromixing, which takes place at the molecular scale, has been considered as the rate determining step during the chemical reaction of particle crystal growth in the reactors, especially for the fast chemical

reactions involved as pointed out by Baldyga and Bourne (1999). A perfect micromixing condition can effectively increase the yield of the desired particle and reduce by-products in the synthesis process at the same time. It should be mentioned that mixing is deemed to be effective at the macro scale, but the mixing may not have dispersed homogeneously at the micro scale yet. Thus, the improvement of micromixing will be beneficial to the synthesis of the particles.

Various kinds of reactors have been developed and investigated in previous studies, aiming to improve the mixing performance. For example, the use of a spinning disk reactor (Jacobsen and Hinrichsen, 2012), impinging jet reactor (Liu *et al.*, 2014), microchannel reactor (Shi *et al.*, 2012), T-shaped reactor (Gao *et al.*, 2015), and high shear mixer (Qin *et al.*, 2017) have all been studied before. The Taylor-Couette (TC) reactor with the features of controllable mean residence time and narrow shear rate distribution has also received a lot of attention. This type of reactor has a simple configuration, where the inner cylinder rotates relative to the outer one. Jung *et al.* (2000) prepared calcium carbonate particles by a gas-liquid reaction system using a TC reactor, and obtained three particle morphologies (cube-like, transition and spindle). They attempted to introduce an enhancement factor in order to characterise this type of behaviour, which is related to the mass transfer rate and suggested that the particle shape change is dependent on this enhancement factor. Tang *et al.* (2019) have investigated the morphology change of copper sulfide nanoparticles by using the TC reactor and they have also found that an intensified mass transfer rate can be achieved using the TC reactor. By tracing the other applications, Haut *et al.* (2003) employed a TC device to culture animal cells and found that the device is more appropriate than a conventional stirred tank in terms of the control of oxygen content and cell suspension. They believed that the adoption of TC reactor can effectively enhance mass transfer rate and create a relatively mild environment for cell growth. Kim and his co-researchers have employed the TC reactor to synthesise many types of fine particles, such as cathode precursors for lithium ion batteries (Mayra and Kim, 2015; Thai *et al.*, 2015; Kim and Kim 2017), barium sulfate (Aljishi *et al.*, 2013), L-histidine (Park and Kim, 2018), and Guanosine 5-monophosphate (Nguyen *et al.*, 2011). Their work mainly focused on the applications of the TC reactor during various particle production processes. However, these studies lacked the fundamental investigation of the mechanisms involved behind the mixing, mass transfer and heat transfer processes.

During particle synthesis processes, many previous studies have indicated that even a minor change of reactor configuration will lead to a significant effect on the micromixing performance. Jacobsen and Hinrichsen (2012) investigated the micromixing characteristics in a spinning disk reactor with different feeding locations and surface structures. In addition, by validation, they synthesised barium sulfate particles with different reactor configurations and obtained various particle morphologies and sizes. Bertrand *et al.* (2016) applied computational fluid dynamics to simulate the micromixing in three types of mixers from the same family but with some geometrical differences: T-shaped tube, Y-shaped tube, and Hartridge-Roughton mixing device. Both experimental and numerical results indicated that the Hartridge-Roughton tube is the most efficient one. Zhu *et al.* (2019) synthesised cathode precursor $\text{Ni}_{0.6}\text{Co}_{0.2}\text{Mn}_{0.2}(\text{OH})_2$ for lithium ion batteries in a stirred tank with four different types of impeller. They finally obtained particles with different shapes and tap densities and consequently, different electrochemical performances. They attributed these differences to the different flow fields generated by four impellers. All these previous studies have revealed that geometrical optimisation is an effective and economical approach to improve the performance of these existing reactors. As mentioned earlier, TC reactor has many features that are beneficial to the particle synthesis due to the fast mass transfer and easy shear control. However, the shear regions in the TC reactor are not locally uniformly distributed. In order to better utilise the advantages of the overall shear control, the modification of the classical TC reactor may improve the features of local turbulent shear. Soos *et al.* (2007) proposed a lobed profile for the inner cylinder in order to reduce the low velocity gradient region. They found that this configuration can successfully enhance the local shear rate in the vicinity of the inner cylinder. Li *et al.* (2015) have compared the mixing performance in the TC reactor with various cross-sectional profiles of inner cylinder including a lobed one using CFD simulation in terms of flow patterns, shear strain rate distribution and micromixing time. They ascertained that the mixing performance improves when using the inner cylinder with a lobed profile. Liu *et al.* (2020) have reported the synthesis of the barium sulfate particles

by using the TC reactor with the classical circular cross-sectional profile inner cylinder and a lobed profile inner cylinder. The experimental results clearly indicate that the properties of the secondary particles are different in terms of particle morphology, particle size and its distribution. The aforementioned investigations have implications where the mixing in the TC reactor is significantly affected by the hydrodynamics in the reactor and also by the inner cylinder configuration adopted.

So far, the micromixing process in the TC reactor has not been clearly understood though a number of experimental work and theoretical studies conducted (Drozdov, 2002; Racina and Kind, 2006; and Richter et al., 2008). Also, these previous studies have mainly focused on the TC reactors with the circular cross-sectional profile inner cylinder and the modifications on the configuration were subjected to the changes of gap size and aspect ratio (DiPrima, 1984; Xiao *et al.*, 2002). The impact of configuration variation on the micromixing performance, especially the inner cylinder alteration, is still rarely studied in the literature.

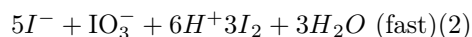
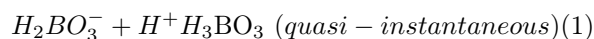
The aim of the present work is to investigate the micromixing performance in the TC reactor with two different types of inner cylinders and to obtain the guidelines for further enhancing the micromixing performance through the modification of the TC reactor configuration. A parallel competing system based on the iodide-iodate reaction proposed by Villermaux and co-workers (Villermaux *et al.*, 1994; Fournier *et al.*, 1996) has been employed, attempting to reveal the effects of key operating parameters on the segregation index, which can reasonably serve as an indicator for assessing the micromixing performance. The key parameters include the Reynolds number based on the gap size, the reactant feeding time and the acid concentration. In addition, the micromixing time based on the experimental data by employing the incorporation model are also evaluated and compared. This paper will be organised as follows. Section 2 will present the theoretical background and modelling details for evaluating the micromixing using the iodide-iodate reaction as the system, while Section 3 will present the experimental details for such chemical probe in the TC reactors with micromixing performance evaluation. Section 4 will present the results and discussion and finally, Section 5 will summarise the conclusions derived from the study.

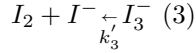
Micromixing characterization modelling

Various chemical reaction schemes serving as molecular probes have been proposed and commonly accepted by researchers to characterise the micromixing performance for the reaction system involved. Typical systems are single reaction systems ($A + B \rightarrow R$), consecutive reaction systems ($A + B \rightarrow R, B + R \rightarrow S$) and parallel competing reaction systems ($A + B \rightarrow R, A + C \rightarrow S$). Due to the rigorous conditions imposed for the on-line analysis of the single reaction, the last two schemes are favoured and usually employed when measuring the final product quality. Bourne and his co-workers proposed several reaction systems based on the consecutive competing scheme, such as the bromination of 1,3,5-trimethoxybenzene (Bourne and Kozicki, 1977), the azo-coupling of 1-naphthol with diazotised sulphanilic acid (Bourne *et al.*, 1981) and the selective iodination of l-tyrosine (Bourne and Rohani, 1983). However, these proposed systems and the experimental methods still have some disadvantages, especially with their toxic, volatile and unstable nature. With a better understanding of the mixing and chemical reactions, Villermaux *et al.* (1994) and Fournier *et al.* (1996) proposed the use of a parallel competing scheme based on the iodide-iodate reaction system. Generally, the products produced in such a system are easily analysed by using the spectrophotometric method. This method have been successfully applied for the assessment of the micromixing efficiency in stirred vessel reactors (Unadkat *et al.*, 2013; and Lemenand *et al.*, 2017) and in high shear mixer (Qin *et al.*, 2017). As the use of the parallel competing reaction system has the advantages of simple control, sensitive measurement through detection of the product concentration and low toxicity of agents, the Villermaux iodide-iodate reaction system is adopted in the present study.

2.1 Reaction kinetics

The reaction system can be described by three sub-reactions, which are expressed as





where H^+ stands for the hydrogen ion of the sulfuric acid (H_2SO_4). Such a system can be regarded as having a competition between the first neutralisation reaction and the second Dushman reaction that produces the by-product of iodine, leading to the occurrence of the third reaction. The concentration of triiodide (I_3^-) in the third reaction can be measured by a UV spectrophotometer. Reaction (1) is quasi-instantaneous with a second-order rate constant k_1 at about $10^{11} \text{ Lmol}^{-1}\text{s}^{-1}$ (Unadkat *et al.*, 2013), while Reaction (2) is very fast and has the same order of magnitude as the micromixing process as indicated by Fournier *et al.* (1996). The rate constant k_2 depends on the ionic strength I (Guichardon *et al.*, 2000) and will change during the micromixing process, which was found to be well approximated by the following empirical relationships:

$$\lg k_2 = 9.28 - 3.66\sqrt{I_i}, \quad I_i < 0.16 \text{ mol} \bullet L^{-1} \quad (4)$$

$$\lg k_2 = 8.38 - 1.51\sqrt{I_i} + 0.23I_i, \quad I_i > 0.16 \text{ mol} \bullet L^{-1} \quad (5)$$

The rate laws of Reactions (1) and (2) can be expressed as

$$r_1 = k_1 c_{H_2BO_3^-} c_{H^+} \quad (6)$$

$$r_2 = k_2 c_{I^-}^2 c_{IO_3^-} c_{H^+}^2 \quad (7)$$

The equilibrium constant K_3 of Reaction (3) is given by

$$K_3 = \frac{k_2}{k_3} = \frac{c_{I_3^-}}{c_{I_2} c_{I^-}} \quad (8)$$

For a given reaction, the value of K_3 is only dependent on temperature. For I_3^- formation, K_3 is given by Palmer *et al.* (1984) and is expressed as follows:

$$\lg K_3 = \frac{555}{T} + 7.355 - 2.575 \log_{10} T \quad (9)$$

Due to these three reactions occurring in one system, there is a material balance on each component. On the basis of yield of iodide ion (i.e., I^-), its material balance can be written as

$$c_{I^-} = \frac{c_{I_0^-} V_1}{V_0 + V_1} - \frac{5}{3} (c_{I_3^-} + c_{I_2}) - c_{I_3^-} \quad (10)$$

where $c_{I_0^-}$ stands for the initial concentration of I^- . V_0 represents the volume of H_2SO_4 solution, while V_1 is the volume of the mixture solution of reactants. H_2SO_4 , serving as the limiting agent, is additionally injected to the system to trigger the parallel competing reaction between Reactions (1) and (2).

Combining Equations (8) and (9) with (10), the concentration of iodine (I_2) can be calculated from Equation (11).

$$-\frac{5}{3} c_{I_2}^2 + \left(\frac{c_{I_0^-} V_1}{V_0 + V_1} - \frac{8}{3} c_{I_3^-} \right) c_{I_2} - \frac{c_{I_3^-}}{K_3} = 0 \quad (11)$$

The main by-product of the Villiermaux iodide-iodate reaction system is I_2 . With the presence of excessive I^- , I_2 will further react with I^- to generate I_3^- until an equilibrium is reached. Since I_3^- will have absorption peaks at the wavelength of 288 nm and 353 nm in the spectrum, the concentration of I_3^- can be measured by a UV spectrophotometer. However, I^- also presents the absorption peak at around 288 nm in the spectrum. In order to reduce interference from the other components, the use of 353 nm as an indicator is preferable for the concentration measurement of I_3^- . According to Beer-Lambert's law, the absorption A of a component across a quartz cell with a thickness Ψ is linearly dependent on its concentration c and molar extinction coefficient e , i.e.

$$A_{353} = e_{353} c_{I_3^-} \Psi. \quad (12)$$

For a particular product and a quartz cell, the molar extinction coefficient e and thickness Ψ are fixed values. Thus, the absorption is linearly dependent on the concentration of I_3^- . The calibration curve of I_3^-

was firstly prepared before experimental work was performed as shown in Figure 1. The calibration curve with R^2 equal to 0.987 highlights that the Beer- Lambert's law is valid within the range of I_3^- concentration chosen in the present study. For the micromixing experiment test, once the absorption of triiodide ion is obtained from the UV spectrophotometer, the concentration of I_3^- can be calculated from the calibration curve.

Definition of segregation index

The segregation index (X_s) is defined as the relative amount of H^+ consumed by Reaction (2). For a perfect micromixing condition, all H^+ would need to be evenly distributed in the system and then immediately consumed by borate ion (i.e., $H_2BO_3^-$) without the appearance of Reaction (2). On the contrary, for poor micromixing, $H_2BO_3^-$ and I^- , iodate ion (i.e., IO_3^-) would compete with H^+ simultaneously. According to stoichiometry, the yield of I_2 from Reaction (2) for a total segregation is expressed as,

$$Y_{ST} = \frac{6n_{IO_3,0^-}}{6n_{IO_3,0^-} + n_{H_2BO_3,0^-}} \quad (13)$$

In practice, I_2 exists in two parts. One is generated in Reaction (2), and the other one is consumed by Reaction (3). Thus, the yield of I_2 should be calculated through the ratio of total mole of both I_2 and IO_3^- to the initial mole of H^+ , as defined by

$$Y = \frac{2(n_{I_2} + n_{I_3^-})}{n_{H_0^+}} \quad (14)$$

Therefore, X_s can be written as

$$X_S = \frac{Y}{Y_{ST}} = \frac{n_{I_2} + n_{I_3^-}}{n_{H_0^+}} \left(2 + \frac{n_{H_2BO_3,0^-}}{3n_{IO_3,0^-}} \right) \quad (15)$$

Equation (15) can be converted in terms of the concentration given by Equation (16).

$$X_S = \frac{(c_{I_2} + c_{I_3^-})V_1}{n_{H_0^+}} \left(2 + \frac{c_{H_2BO_3,0^-}}{3c_{IO_3,0^-}} \right) \quad (16)$$

By definition, the value of X_S varies between 0 and 1 with a lower value indicating a better micromixing performance.

$X_s = 0$ Perfect micromixing $X_s = 1$ Total segregation $0 < X_s < 1$ Partial segregation

CFD modelling

In order to get a better understanding of the mixing conditions in the TC reactor, the flow fields of two different inner cylinders were simulated using commercial CFD code, FLUENT 17.0. Based on the structures of the two types of inner cylinder shown in Figure 2, the geometry was created by ANSYS ICEM. Then, the computational domain was divided into two zones, connected by the predefined interface. The total meshes have around 1,100,000 cells, with each direction of $16 \times 147 \times 480$ (radial \times circumferential \times axial). Our previous work (Liu *et al.*, 2020) presents the details for such flow field simulation, where RNG k- ϵ turbulent model was adopted. The boundary conditions were set as velocity inlet and pressure outlet with no slip wall. The discretized equations were realized by the SIMPLEC algorithm.

Experimental work

3.1 Apparatus setup

The apparatus of the Taylor-Couette reactor is illustrated in Figure 2(a). Two types of inner cylinder are adopted in this study, one being the classical inner cylinder with a circular cross-sectional profile and the other is a lobed cross-sectional profile inner cylinder, whose cross section consists of three identical arcs connected by three tangential lines. Figure 2(b) displays the cross-sectional profiles for both geometries. Here, the

abbreviations of CTC and LTC denote the classical Taylor-Couette reactor and the lobed Taylor-Couette reactor, respectively. The dimensions of the TC reactor are described in Table 1.

Table 1. Dimensions of the TC reactor.

Dimension	CTC	LTC
Reactor length, L (mm)	300.00	300.00
Outer cylinder radius, r_o (mm)	50.00	50.00
Inner cylinder radius (original or equivalent), r_i (mm) Gap size, d (mm)	40.00 10.00	40.19 9.81

In order to determine the flow pattern in the TC reactor, the Reynolds number based on the gap size has been adopted, as defined by

$$Re = \frac{\omega_i r_i d}{\nu} \quad (17)$$

where ω_i and r_i are the angular velocity and the radius of the inner cylinder, respectively. d is the gap size, and ν is the kinematic viscosity of the suspension. In this study, various cases with different Reynolds number have been investigated by changing the rotational speed of the inner cylinder. The critical Reynolds number (Re_c), which indicates the presence of Taylor vortex flow was found to be about 97 with the classical inner circular cylinder (i.e., radius ratio $\eta = \frac{r_i}{r_o} = 0.8$). When the Reynolds number exceeds the critical Reynolds number, the flow pattern will experience a series of instabilities, including wavy Taylor vortex flow and turbulent Taylor vortex flow, which can finally develop into turbulent Taylor flow (Grossmann *et al.*, 2016).

3.2 Villermaux reaction procedures

All the agents were purchased from Sinopharm Chemical Reagent Co., Ltd of China with a purity level of above 99.0%. The reactor gap was filled with the mixture solution of boric acid (H_3BO_3 , 0.089 mol/L), potassium iodide (KI, 0.0116 mol/L), potassium iodate (KIO_3 , 0.00233 mol/L), and sodium hydroxide (NaOH) with deionised water. NaOH was used to adjust the pH value around 10.0 in order to prevent the reaction between KI and KIO_3 with the presence of H^+ . Therefore, the pH value should be carefully controlled during solution preparation.

The rotational speed was adjusted within the range of 50 rpm to 1000 rpm, corresponding to the Reynolds Number varying from 2000 to 42000. After the system reached a steady state, H_2SO_4 solution was injected into the reactor from the bottom inlet. In each run, about 3 mL of sample solution was collected for the UV test from the top outlet after completing the mixing. The absorption intensity test was conducted immediately using the UV spectrophotometer (UNICO SQ4802 UV/VIS Spectrophotometer, U.S.A) at the wavelength of 353 nm to ensure the stability of I_3^- . The experiment and the sample measurement were carried out at the room temperature of 25. The operating conditions are summarised in Table 2.

Table 2. Operating conditions.

Experimental number	Feeding time (s)	H^+ concentration (mol/L)	Rotational speed (rpm)	Reynolds
R1	120	2.0	50	2094
R2	120	2.0	100	4188
R3	120	2.0	200	8376
R4	120	2.0	300	12564
R5	120	2.0	400	16752
R6	120	2.0	600	25128
R7	120	2.0	800	33504
R8	120	2.0	1000	41880
R9	20	2.0	300	12564

Experimental number	Feeding time (s)	H ⁺ concentration (mol/L)	Rotational speed (rpm)	Reynolds
R10	40	2.0	300	12564
R11	60	2.0	300	12564
R12	90	2.0	300	12564
R13	240	2.0	300	12564
R14	360	2.0	300	12564
R15	480	2.0	300	12564
R16	120	1.2	300	12564
R17	120	1.6	300	12564
R18	120	4.0	300	12564
R19	120	5.0	300	12564
R20	120	6.0	300	12564

Results and discussion

In the segregation experiments, the sampling location was set with a distance away from the inlet of acid injection. In order to guarantee that a well-established micromixing process is achieved throughout the whole reactor, the collection time after acid injection should be determined in advance. The preliminary experiment was performed at a Reynolds number of 12564 in the CTC. It can be seen from Figure 3 that the critical collection time is 120 s after finishing the injection of acid. However, within the range from 90 s to 240 s, the results used to determine the collection time also appear to be acceptable. One can argue that if the collection time is too short, the macromixing has not been fully achieved, thus resulting in little amount of the product being detected at the outlet. On the other hand, if the collection time is too long, the UV result may lose its accuracy since I_3^- is very sensitive to light. Therefore, the determination of the critical collection time is crucial for acquiring reliable results. It should be noted that for different operating conditions, the critical collection time may be different within the acceptable range. The following discussion on the micromixing in the TC reactor with two different inner cylinder configurations will be based on the samples collected at the critical collection time determined for the CTC and LTC, respectively.

4.1 Effect of feeding time on X_s s

Mixing in the TC reactor involves all the scales from macro-scale, meso-scale to micro-scale. In order to better separate the influence of macromixing on micromixing and only observe the micromixing behavior, the feeding rate of acid solution should be controlled as low as possible as mentioned earlier. In our experiment, the injection of acid solution was maintained at a constant feeding rate, which means the feeding time should be controlled long enough.

Figure 4 shows the change of X_s with feeding time in the CTC and LTC, where X_s gradually decreases and reaches an almost constant value with little fluctuation. When taking a very fast injection, the value of X_s will be jointly controlled by both macro- and micro-mixing. Under such a condition, the local concentration gradient can be very high, as the acid plume cannot be dispersed well throughout the whole reactor scale (Baldyga & Bourne, 1999). Accordingly, this will lead to the local excess of H⁺ and a large value of X_s . However, this is mainly caused by poor dispersion rather than poor micromixing in the reactor, as the effect of macromixing is not eliminated. On the other hand, a fast injection leading to a random fluctuation will break the steady state of flow field. When more turbulent eddies are involved, the dynamic balance of acid engulfment with bulk reactants cannot be achieved. As local $H_2BO_3^-$ is not enough to consume a large amount of H⁺, the excessive H⁺ will react with I^- and IO_3^- , yielding a large value of X_s . With a slow injection of acid, the turbulence is less affected such that the acid has enough time to be dispersed evenly in a macro-scale in the reactor and a well-established environment for micromixing is obtained. Consequently, the UV measurement result given by chemical test reactions is free from the macromixing influence and is only dependent on the micromixing behavior. Thus, the feeding time of 120 s was chosen for all the subsequent experiments.

4.2 Effect of H^+ concentration on X_s

Because the linear relationship between I_3^- concentration and its absorption is valid within a particular range, the H^+ concentration should be selected appropriately to avoid excessive or too little I_2 being generated. A wide range of H^+ concentration from 1.2 mol/L to 6.0 mol/L has been tested. The experiment was conducted under the condition of the Reynolds number of 12564 with 1.0 mL injection. It can be seen from Figure 5 that the value of X_s firstly increases, then levels off with the increase of H^+ concentration. At a higher H^+ concentration, more time is needed for $H_2BO_3^-$ to neutralize H^+ . However, the amount of $H_2BO_3^-$ was kept at a constant level when changing the H^+ concentration. Thus, the excessive H^+ will lead to the occurrence of Reaction (2). It can be seen from the rate laws of (6) and (7) that Reaction (2) is sensitive to H^+ due to its higher rate order. Moreover, the chemical reaction rate of Reaction (2) is usually higher if measured based on the micromixing rate (Fournier *et al.*, 1996), which will be presented and discussed in Section 4.4. It can be seen that a large amount of I_2 is generated, leading to a high value of X_s . It is worth mentioning that the continuous increase of H^+ concentration does not give rise to the continuous increase of X_s . Due to the local excess of H^+ concentration, both Reactions (1) and (2) have been completed, which means that all reactants have achieved their maximum conversion. As a result, the I_2 concentration will not increase any further. It can also be seen from Figure 5 that the most sensitive point for the UV detection corresponds to the H^+ concentration of 2.0 mol/L. This value has been chosen for all the subsequent experiments.

One can see from Figure 5 that the micromixing X_s in the LTC is better than that of the CTC at all ranges of the H^+ concentration, but such a difference is less noticeable at high H^+ concentration. For the LTC, the rotational lobed inner cylinder generates a periodic variation of the gap size. The circumferential flow will experience an expansion and contraction, leading to the generation of the induced turbulent eddies from the surface of the concaved top of the inner cylinder and the enhanced turbulent eddy interactions. Such turbulent eddy interaction can effectively re-disperse the concentration field of reactants, promoting a better distribution of the reactants, less local H^+ accumulation and less local formation of I_2 . This is another piece of evidence to suggest that lobed geometry can effectively reduce the overall mixing time and improve the micromixing efficiency for the TC reactor.

4.3 Effect of Reynolds number on X_s

Figure 6 (a) shows the effect of the variation of Reynolds number on X_s under the condition of 1.0 mL sulfuric acid solution injected within 120 s. With the increase of Reynolds number, X_s decreases in both the CTC and LTC. When Reynolds number is greater than 25128 (corresponding to 600 rpm), the decrease in X_s becomes small. At a low rotational speed, i.e., a small Reynolds number, X_s presents a very high value, and the difference between the CTC and LTC is very small, which can be attributed to the excessive turbulence generated by the lobed inner cylinder being still small. Although the geometry modification can enhance the micromixing to some extent, flow pattern has not become fully turbulent for both the CTC and LTC. The degree of the occurrence of the micromixing may still rely on the molecule-scaled diffusion. The reactant fluid elements that contribute to the micromixing still hold a relatively large size compared with the molecular diffusion length scale. In such case, the micromixing may not be sufficient. With the increase of Reynolds number, turbulence intensity is gradually built up and the flow in the reactor develops to the turbulent state, and the micromixing improves evidenced by drop in X_s . Although the chemical reaction occurs at molecular level, the intensified turbulence can provide the environment for reactant fluid elements to break into much smaller size eddies with the surface area for the mass transfer being increased. As a result, mixing diffusion improves and the micromixing rate can be accelerated. Finally, as Reynolds number exceeds 25128, it was observed that X_s levels off, reaching a minimum of about 0.15 and 0.08 for the CTC and LTC, respectively.

We cautiously mention here that the difference of X_s between the CTC and LTC becomes remarkable with the flow in the TC reactor to be judged to be fully turbulent. The LTC shows a much better micromixing than the CTC. This may be explained by the facts: Firstly, with the rotation of the inner cylinder, gap size of the LTC varies periodically so that the formed Taylor vortices change and the vortices are deformed. Consequently, this type of perturbation due to the deformation Taylor vortices will induce the generation

of small turbulent eddies down to the scales beneficial to the micromixing. Secondly, Liu *et al.* , (2020) have compared the turbulent flows generated by the CTL and LTC and shown that the impinging jet region existing between the two toroidal counter-rotating Taylor vortices induces a stronger outward shear gradient in the LTC than that in CTL when the same rotational speed was taken. Thus, it can be claimed that the reactant micro elements entrapped by the turbulent eddies generated by the impinging jet flow shear in the LTC can have a shorter entrainment time than the CTC.

In order to quantitatively describe how X_s changes with the Reynolds number, the following relation is proposed, given by

$$X_s = CRe^b \quad (18)$$

By taking the logarithmic transformation of both sides, a liner relationship is obtained. Using this regression fitting, it was found that well fitted relation for the CTC is $\ln X_s = -0.451 \ln Re + 2.963$ with $R^2 = 0.968$ and the same fitted relation for the LTC is $\ln X_s = -0.635 \ln Re + 4.319$ with $R^2 = 0.986$, respectively. As the slopes b for both relations show negative values, the smaller value of b indicates X_s to be more sensitive to turbulent eddies.

As the turbulent intensity can be used to determine the micromixing efficiency as suggested by Qin *et al.* , (2017), the turbulent intensity measured on the surface of the inner cylinder for both the CTC and LTC based on CFD simulation is shown in Figure 7. For three representative rotational speeds, 100, 600 and 1000 rpm, the corresponding Reynolds numbers are 4188, 25128 and 41880, respectively. It can be seen clearly from the figure that the turbulent intensity is enhanced with the increase of Reynolds number for both the CTC and LTC but the enhancement for the LTC is significantly larger than that in the CTC. Also, the highest turbulent intensity appears at regions of three concaved arcs, corresponding to the smallest gap regions in the LTC. We postulate that the best micromixing may happen in these regions. To demonstrate this, the correlation between the turbulence intensity and $1/X_s$ is proposed.

$$R_{IX_s} = I \frac{1}{X_s} \quad (19)$$

where $\langle I \rangle$ and $\langle X_s \rangle$ are the volume average turbulence intensity and X_s in the reactor. Figure 8 shows such correlation, clearly indicating that the micromixing can be improved through the modification of the inner cylinder configuration of the TC reactor.

4.4 Characterisation of micromixing time

In order to compare the micromixing efficiency of the adopted TC reactor especially the lobed inner cylinder with conventional stirred tank, the micromixing times for different reactors are evaluated. Many models have been proposed to estimate the micromixing time. Among these models, the IEM model (Costa and Trevissoi, 1972), the EDD model (Baldyga and Bourne, 1984), the E-model (Baldyga and Bourne, 1989), and the incorporation model (Villermoux *et al.* , 1994) are representatives. However, the incorporation model has been widely used and recognized as illustrated in Figure 9. This model assumes that the limited agent, acid occupying Environment 2, is divided into several aggregates, which then are progressively invaded by surrounding solution from Environment 1. Consequently, the volume of acid aggregates gradually grows due to the incorporation, based on $V_2 = V_{20}g(t)$. The characteristic incorporation time is assumed to be equivalent to the micromixing time. Fournier *et al.* (1990) proposed a dilution-reaction equation in the reaction Environment 2, which is found to be suitable for the description of the present employed TC reactor system, given by

$$\frac{dc_j}{dt} = (c_{j10} - c_j) \frac{1}{g} \frac{dg}{dt} + r_j \quad (20)$$

where c_j is the reactant concentration, and species j denotes $H_2BO_3^-$, H^+ , I^- , IO_3^- , I_2 , and I_3^- . c_{j10} is the concentration of surrounding solution (i.e., the initial concentration of species j in Environment 1). r_j is the net production rate of species j , and g denotes the mass exchange rate between reactant fluid particle and its surrounding solution. A large value of dg/dt indicates a fast dilution, indicating a good mixing performance

between the feeding acid and its surrounding solution. The empirical equation of the growing law for acid aggregates can be expressed as an exponential function of micromixing time, t_m , which reads

$$g(t) = \exp\left(\frac{t}{t_m}\right) \quad (21)$$

Thus, Equation (20) can be converted into the following form,

$$\frac{dc_j}{dt} = \frac{c_{j10} - c_j}{t_m} + r_j \quad (22)$$

From Equation (22), the mass balance equation of individual species can be obtained. In total, there are six transport equations to be solved. In order to reduce computational cost, the W-Z transformation was adopted to reduce the number of solutions and the simplification yields

$$\frac{dW}{dt} = -\frac{c_{H_2BO_3^-}, 10 + W}{t_m} - 6r_2 \quad (23)$$

$$\frac{dY}{dt} = \frac{c_{I^-}, 10 - Y}{t_m} - 8r_2 \quad (24)$$

$$\frac{dZ}{dt} = \frac{c_{I^-}, 10 - Z}{t_m} - 5r_2 \quad (25)$$

$$\frac{dc_{IO_3^-}}{dt} = \frac{c_{IO_3^-}, 10 - c_{IO_3^-}}{t_m} - r_2 \quad (26)$$

where $W = c_{H^+} - c_{H_2BO_3^-}$, $Y = c_{I^-} - c_{I_2}$, and $Z = c_{I^-} + c_{I_3^-}$. Equations (23)-(26) can be solved numerically by iteration, where the initial conditions are given by $W = c_{H^+}, 0$, $Y = 0$, $Z = 0$, and $c_{IO_3^-} = 0$. The iteration ends as H^+ concentration approaches 0. Acid concentration reaches its highest value at the inlet, then, it disperses within a very limited range and is consumed quickly. Thus, H^+ concentration is assumed to be at its initial value, $c_{H^+}, 0$ during the iteration before it is completely consumed. The fourth-order Runge-Kutta method was adopted in the present study to calculate t_m . Firstly, a series value of t_m is assumed. Following the Runge-Kutta iteration, Equations (23)-(26) are solved, and the concentration of individual species are obtained. Subsequently, a set of segregation index Xs can be calculated based on Equation (16). Figure 10 depicts the obtained relation of Xs against the micromixing time t_m ($Xs = 37991 t_m$) based on fitting the calculated values of Xs . This relation can be used to evaluate the micromixing time in TC reactor based on the value of Xs obtained from the experimental results, which are also shown in Figure 10. Figure 11 shows the relationship between the Reynolds number and micromixing time in the CTC and LTC. For better description, the contour of turbulent intensities in the circumferential direction for both the CTC and LTC is also shown in Figure 10, where the intensified regions by geometry modification can be seen clearly. By using power law fitting, the micromixing time for both the CTC and LTC can be approximated by $t_m = 0.0025Re^{-0.664}$ and $t_m = 0.0006Re^{-0.456}$, respectively.

Damköhler number (Da), defined as the ratio of the chemical reaction timescale (reaction rate) to the mixing timescale (mixing rate), is also used to characterize the impact of hydrodynamics in the TC reactor on chemical reaction. Here, we use the obtained relations for the micromixing time to estimate Da_1 and Da_2 for Reactions (1) and (2), respectively. The chemical reaction time for Reactions (1) and (2) is given by

$$t_{r1} = \frac{\min(c_{H_2BO_3^-}, 0; c_{H^+}, 0)}{r_1} \quad (27)$$

$$t_{r2} = \frac{\min(\frac{3}{5}c_{I^-}, 0; 3c_{IO_3^-}, 0; \frac{1}{2}c_{H^+}, 0)}{r_2} \quad (28)$$

Thus, Da_1 and Da_2 can be estimated using Equations (29) and (30).

$$Da_1 = \frac{t_m}{t_{r1}} = t_m k_1 c_{H^+}, 0 \quad (29)$$

$$Da_2 = \frac{t_m}{t_{r2}} = t_m k_2 c_{I^-}, 0^2 c_{H^+}, 0^2 \quad (30)$$

The estimated $Da_1 = 4.2 \times 10^5 - 2.8 \times 10^6$ is much greater than 1, indicating that Reaction (1) is an instantaneous reaction. $Da_2 = 3.2 \times 10^{-3} - 2 \times 10^{-2}$ has the order of 10^{-2} , which is small than 1. Both results indicate that the

iodide-iodate reaction system used for evaluation of the micromixing performance in the TC reactor to be suitable.

Compared with the conventional stirred tank reactor, in which the micromixing time is the order of 20 ms (Fournier *et al.*, 1996), the order of micromixing time in the TC reactor is evaluated to be 10^{-5} s based on the above discussion. It thus can be claimed that the TC reactor can have a better micromixing performance than the traditional stirred tank reactor as far as those fast chemical processes controlled by the mixing are concerned. The use of the lobed inner cylinder configuration in the TC reactor can further shorten the micromixing time due to the local turbulence intensification.

Conclusions

The micromixing performance in a TC reactor with two different inner cylinder geometries has been evaluated based on the parallel competing iodide-iodate reaction system to characterise the impact of the inner cylinder configuration variations on the micromixing process that will significantly affect the hydrodynamic environment of the particle synthesis. Segregation index X_s was employed as an indicator to characterise the micromixing efficiency. In order to assess the effects of various factors, the sample collection time has been carefully determined to ensure the reliable UV results. The acid concentration was also carefully chosen to avoid over-loading, while the injection of acid was controlled to keep the feeding as slow as possible in order to eliminate the impact on the macromixing in the TC reactor. The conclusions reached for the present study can be summarised as follows:

- (1) The segregation experimental results have indicated that the value of X_s decreases with the increase of Reynolds number for both inner cylinder configurations but the LTC exhibits a better micromixing performance than the CTC as X_s for the LTC is smaller than the CTC.
- (2) CFD simulation results have revealed that the turbulence shear generated in the jet regions in vicinity of the inner cylinder of the LTC is stronger than that of the CTC, which subsequently enhances the local micromixing, which can be characterised by the enhancement of the turbulence intensity in these regions close to the inner cylinder surface. This clearly indicates that the modification of the inner cylinder configuration (here, the use of a lobed cross-sectional profile) may improve the micromixing action significantly.
- (3) Predictions made by employing the incorporation model show that the micromixing time is estimated to be of the order of 10^{-5} s for the TC reactor, much smaller than that of the traditional stirred tank reactor according to the open literature. In addition, the LTC shows a shorter micromixing time than the CTC.

Nomenclature

A_{353}	absorption at 353 nm	c_j	concentration of species j, mol/L
d	gap width, m	e_{353}	Damköhler number
g	molar extinction coefficient, L/mol/mm	I_i	growing rate for incorporation
k	reaction rate constant, m^2/s^2 , dimension dependent on reaction order	K_3	equilibrium constant for Reaction (3)
L	reactor length, m	n_j	mole of species j, mol
r	chemical reaction rate, mol/L/s	r_i	radius of the inner cylinder, m
r_o	radius of the lobed outer cylinder, m	Re	Reynolds number
R_{IX_s}	Reynolds number correlation	t_m	micromixing time, s
t_r	chemical reaction time, s	T	thermodynamic temperature, K
Y	segregation index	Y	yield of iodine

Greek letters

ν	kinematic viscosity of the fluid, m^2/s
ω_i	rotational speed of the inner cylinder, rad/s
Ψ	thickness of quartz cell, mm

Acknowledgement

This work was carried out at the International Doctoral Innovation Centre (IDIC), UNNC. The authors acknowledge the financial support by National Natural Science Foundation of China (NSFC) through the grant (Nos. 21576141, 21606259). The authors also would like to thank the reviewers for their expert guidance on revising the manuscript of this paper.

References

- Aljishi, M.F., Ruo, A.C., Park, J.H., Nasser, B., Kim, W.S. and Joo, Y.L., 2013. Effect of flow structure at the onset of instability on barium sulfate precipitation in Taylor–Couette crystallizers. *Journal of crystal growth* , 373 , pp.20-31.
- Baldyga, J. and Bourne, J.R., 1984. A fluid mechanical approach to turbulent mixing and chemical reaction part II micromixing in the light of turbulence theory. *Chemical Engineering Communications* , 28 (4-6), pp.243-258.
- Baldyga, J. and Bourne, J.R., 1989. Simplification of micromixing calculations. I. Derivation and application of new model. *The Chemical Engineering Journal* , 42 (2), pp.83-92.
- Baldyga, J. and Bourne, J.R., 1999. *Turbulent mixing and chemical reactions* . Wiley.
- Bertrand, M., Lamarque, N., Lebaigue, O., Plasari, E. and Ducros, F., 2016. Micromixing characterisation in rapid mixing devices by chemical methods and LES modelling. *Chemical Engineering Journal* , 283 , pp.462-475.
- Bourne, J.R., 1977. MIXING EFFECTS DURING THE BROMINATION OF 1, 3, 5-TRIMETHOXYBENZENE. *Chemical Engineering Science* , 32 (12), pp. 1538-1539.
- Bourne, J.R., Kozicki, F. and Rys, P., 1981. Mixing and fast chemical reaction—I: Test reactions to determine segregation. *Chemical Engineering Science* , 36 (10), pp.1643-1648.
- Bourne, J.R. and Rohani, S., 1983. Micro-mixing and the selective iodination of l-tyrosine. *Chemical engineering research and design* , 61 (5), pp.297-302.
- Costa, P. and Trevissoi, C., 1972. Reactions with non-linear kinetics in partially segregated fluids. *Chemical Engineering Science* , 27 (11), pp.2041-2054.
- DiPrima, R.C., Eagles, P.M. and Ng, B.S., 1984. The effect of radius ratio on the stability of Couette flow and Taylor vortex flow. *The Physics of fluids* , 27 (10), pp.2403-2411.
- Drozdov, S.M., 2002. A numerical investigation of a modified Couette-Taylor apparatus with application to industrial mixing. *Theoretical and computational fluid dynamics* , 16 (1), pp.17-28.
- Fournier, M.C., Falk, L. and Villermaux, J., 1996. A new parallel competing reaction system for assessing micromixing efficiency—experimental approach. *Chemical Engineering Science* , 51 (22), pp.5053-5064.
- Fournier, M.C., Falk, L. and Villermaux, J., 1996. A new parallel competing reaction system for assessing micromixing efficiency—determination of micromixing time by a simple mixing model. *Chemical Engineering Science* , 51 (23), pp.5187-5192.
- Gao, Z., Han, J., Bao, Y. and Li, Z., 2015. Micromixing efficiency in a T-shaped confined impinging jet reactor. *Chinese Journal of Chemical Engineering* , 23 (2), pp.350-355.
- Grossmann, S., Lohse, D. and Sun, C., 2016. High-reynolds number taylor-couette turbulence. *Annual review of fluid mechanics* , 48 , pp.53-80.
- Guichardon, P. and Falk, L., 2000. Characterisation of micromixing efficiency by the iodide–iodate reaction system. Part I: experimental procedure. *Chemical Engineering Science* , 55 (19), pp.4233-4243.

- Haut, B., Amor, H.B., Coulon, L., Jacquet, A. and Halloin, V., 2003. Hydrodynamics and mass transfer in a Couette–Taylor bioreactor for the culture of animal cells. *Chemical engineering science* , 58 (3-6), pp.777-784.
- Jacobsen, N.C. and Hinrichsen, O., 2012. Micromixing efficiency of a spinning disk reactor. *Industrial & engineering chemistry research* , 51 (36), pp.11643-11652.
- Jung, W.M., Kang, S.H., Kim, W.S. and Choi, C.K., 2000. Particle morphology of calcium carbonate precipitated by gas–liquid reaction in a Couette–Taylor reactor. *Chemical engineering science* , 55 (4), pp.733-747.
- Kim, J.E. and Kim, W.S., 2017. Synthesis of Core–Shell Particles of Nickel–Manganese–Cobalt Hydroxides in a Continuous Couette–Taylor Crystallizer. *Crystal Growth & Design* , 17 (7), pp.3677-3686.
- Lemenand, T., Della Valle, D., Habchi, C. and Peerhossaini, H., 2017. Micro-mixing measurement by chemical probe in homogeneous and isotropic turbulence. *Chemical Engineering Journal* , 314 , pp.453-465.
- Li, G., Yang, X. and Ye, H., 2015. CFD simulation of shear flow and mixing in a Taylor–Couette reactor with variable cross-section inner cylinders. *Powder Technology* , 280 , pp.53-66.
- Liu, Z., Guo, L., Huang, T., Wen, L. and Chen, J., 2014. Experimental and CFD studies on the intensified micromixing performance of micro-impinging stream reactors built from commercial T-junctions. *Chemical Engineering Science* , 119 , pp.124-133.
- Liu, L., Yang, X., Li, G., Huang, X. and Xue, C., 2020. Shear controllable synthesis of barium sulfate particles using lobed inner cylinder Taylor–Couette flow reactor. *Advanced Powder Technology* , 31(3), pp.1088-1099.
- Mayra, Q.P. and Kim, W.S., 2015. Agglomeration of Ni-Rich hydroxide in reaction crystallization: Effect of Taylor vortex dimension and intensity. *Crystal Growth & Design* , 15 (4), pp.1726-1734.
- Nguyen, A.T., Kim, J.M., Chang, S.M. and Kim, W.S., 2011. Phase Transformation of Guanosine 5-Monophosphate in Continuous Couette–Taylor Crystallizer: Experiments and Numerical Modeling for Kinetics. *Industrial & engineering chemistry research* , 50 (6), pp.3483-3493.
- Palmer, D.A., Ramette, R.W. and Mesmer, R.E., 1984. Triiodide ion formation equilibrium and activity coefficients in aqueous solution. *Journal of solution chemistry* , 13 (9), pp.673-683.
- Park, S. and Kim, W.S., 2018. Influence of fluid motions on polymorphic crystallization of L-histidine: Taylor vortex flow and turbulent Eddy flow. *Crystal Growth & Design* , 18 (2), pp.710-722.
- Racina, A. and Kind, M., 2006. Specific power input and local micromixing times in turbulent Taylor–Couette flow. *Experiments in fluids* , 41 (3), pp.513-522.
- Richter, O., Hoffmann, H. and Kraushaar-Czarnetzki, B., 2008. Effect of the rotor shape on the mixing characteristics of a continuous flow Taylor-vortex reactor. *Chemical Engineering Science* , 63 (13), pp.3504-3513.
- Qin, H., Zhang, C., Xu, Q., Dang, X., Li, W., Lei, K., Zhou, L. and Zhang, J., 2017. Geometrical improvement of inline high shear mixers to intensify micromixing performance. *Chemical Engineering Journal* , 319 , pp.307-320.
- Shi, X., Xiang, Y., Wen, L.X. and Chen, J.F., 2012. CFD analysis of flow patterns and micromixing efficiency in a Y-type microchannel reactor. *Industrial & engineering chemistry research* , 51 (43), pp.13944-13952.
- Soos, M., Wu, H. and Morbidelli, M., 2007. Taylor–Couette unit with a lobed inner cylinder cross section. *AIChE journal* , 53 (5), pp.1109-1120.
- Tang, Z., Kim, W.S. and Yu, T., 2019. Studies on morphology changes of copper sulfide nanoparticles in a continuous Couette–Taylor reactor. *Chemical Engineering Journal* , 359 , pp.1436-1441.

Thai, D.K., Mayra, Q.P. and Kim, W.S., 2015. Agglomeration of ni-rich hydroxide crystals in taylor vortex flow. *Powder Technology* , 274 , pp.5-13.

Unadkat, H., Nagy, Z.K. and Rielly, C.D., 2013. Investigation of turbulence modulation in solid–liquid suspensions using parallel competing reactions as probes for micro-mixing efficiency. *Chemical Engineering Research and Design* , 91 (11), pp.2179-2189.

Villermaux, J., Falk, L. and Fournier, M.C., 1994. Potential use of a new parallel reaction system to characterize micromixing in stirred reactors. In *AIChE Symposium Series 90* (299), pp. 50-54.

Villermaux, J. and Falk, L., 1994. A generalized mixing model for initial contacting of reactive fluids. *Chemical Engineering Science* , 49 (24), pp.5127-5140.

Xiao, Q., Lim, T.T. and Chew, Y.T., 2002. Second Taylor vortex flow: Effects of radius ratio and aspect ratio. *Physics of Fluids* , 14 (4), pp.1537-1539.

Zhu, Q., Xiao, H., Zhang, R., Geng, S. and Huang, Q., 2019. Effect of impeller type on preparing spherical and dense Ni_{1-x}Co_xMn_y(OH)₂ precursor via continuous co-precipitation in pilot scale: A case of Ni_{0.6}Co_{0.2}Mn_{0.2}(OH)₂. *Electrochimica Acta* , 318 , pp.1-13.

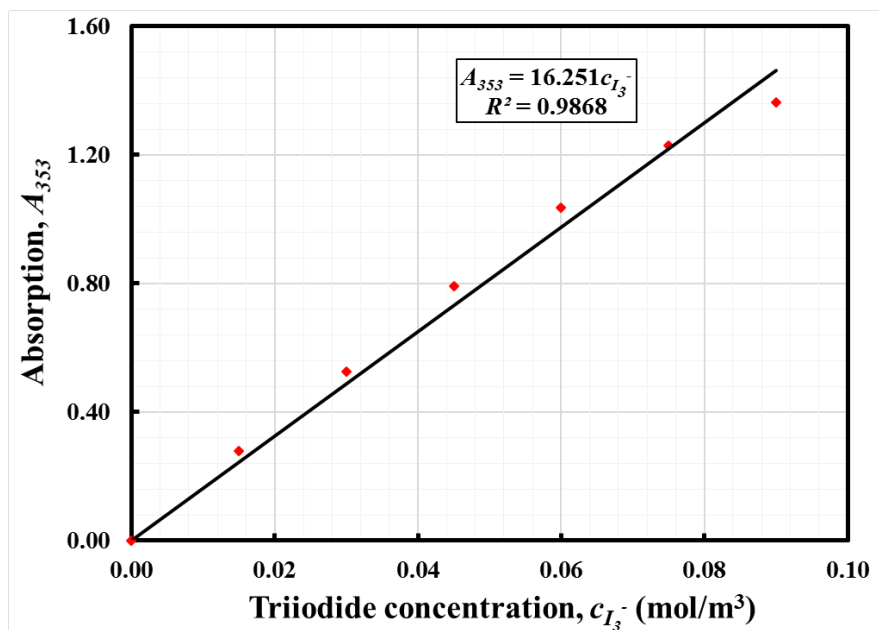
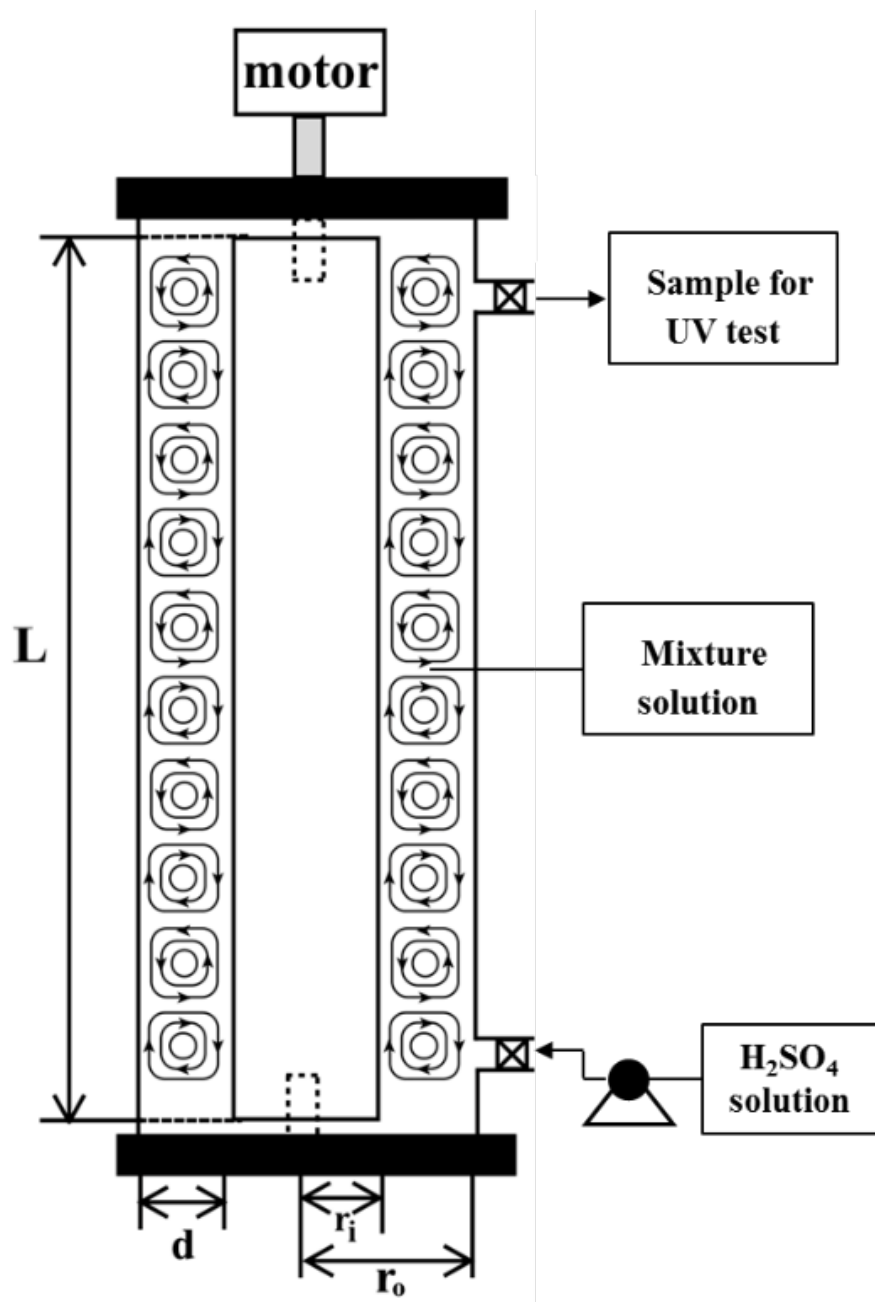
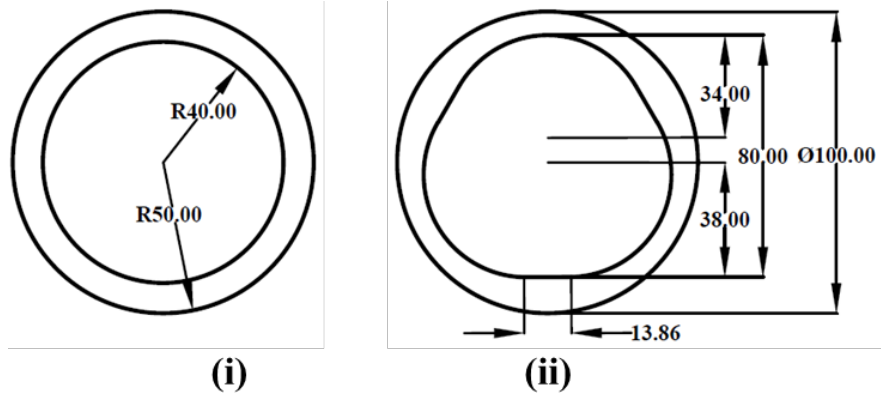


Figure 1. Calibration curve of the triiodide ion concentration at 353 nm in the UV spectrum.





(a) (b)

Figure 2. (a) Schematic diagram of experimental setup; and (b) Schematic of cross-section profiles for TC reactor: (i) CTC; and (ii) LTC.

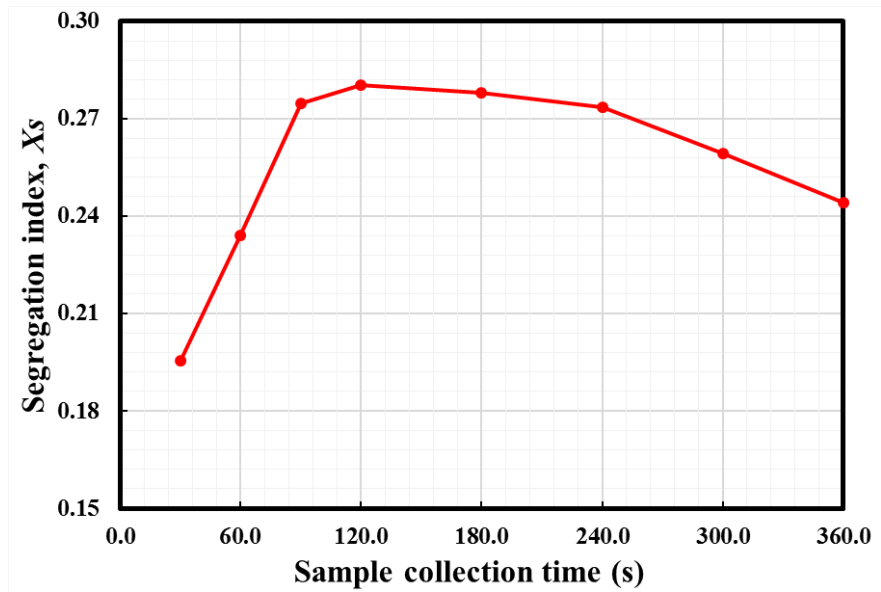


Figure 3. Preliminary test of the selection of sample collection time.

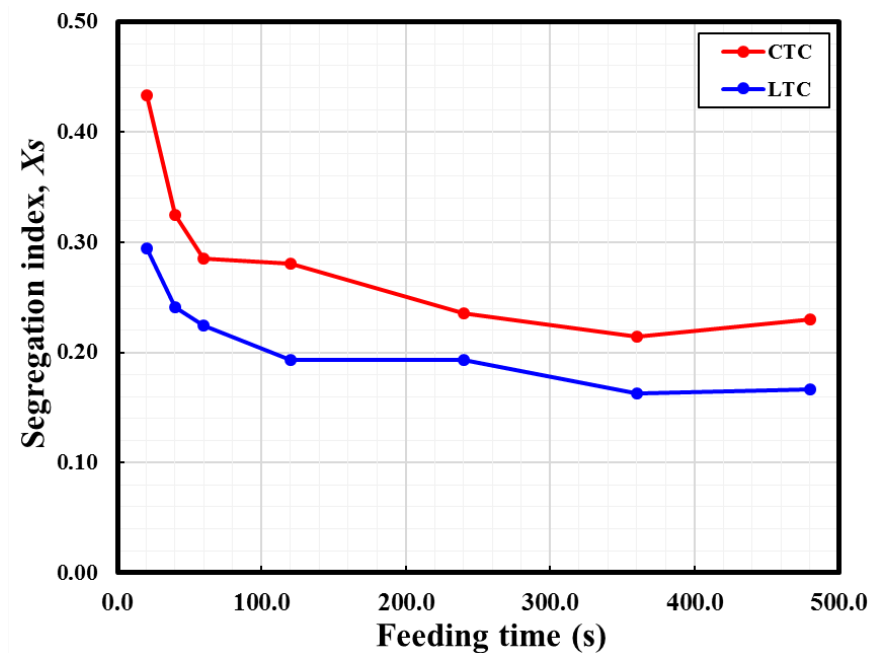


Figure 4. Effect of feeding time on segregation index.

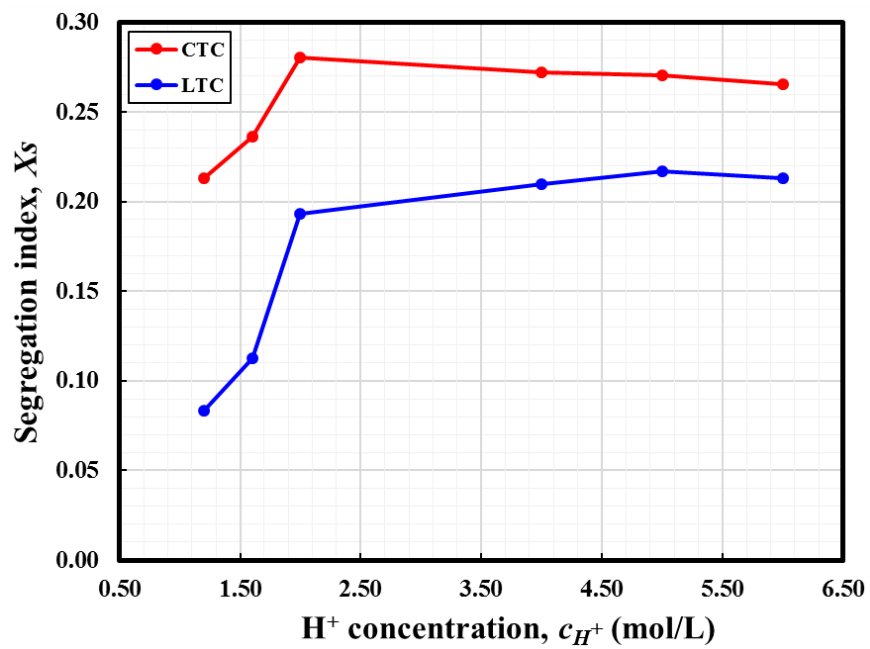
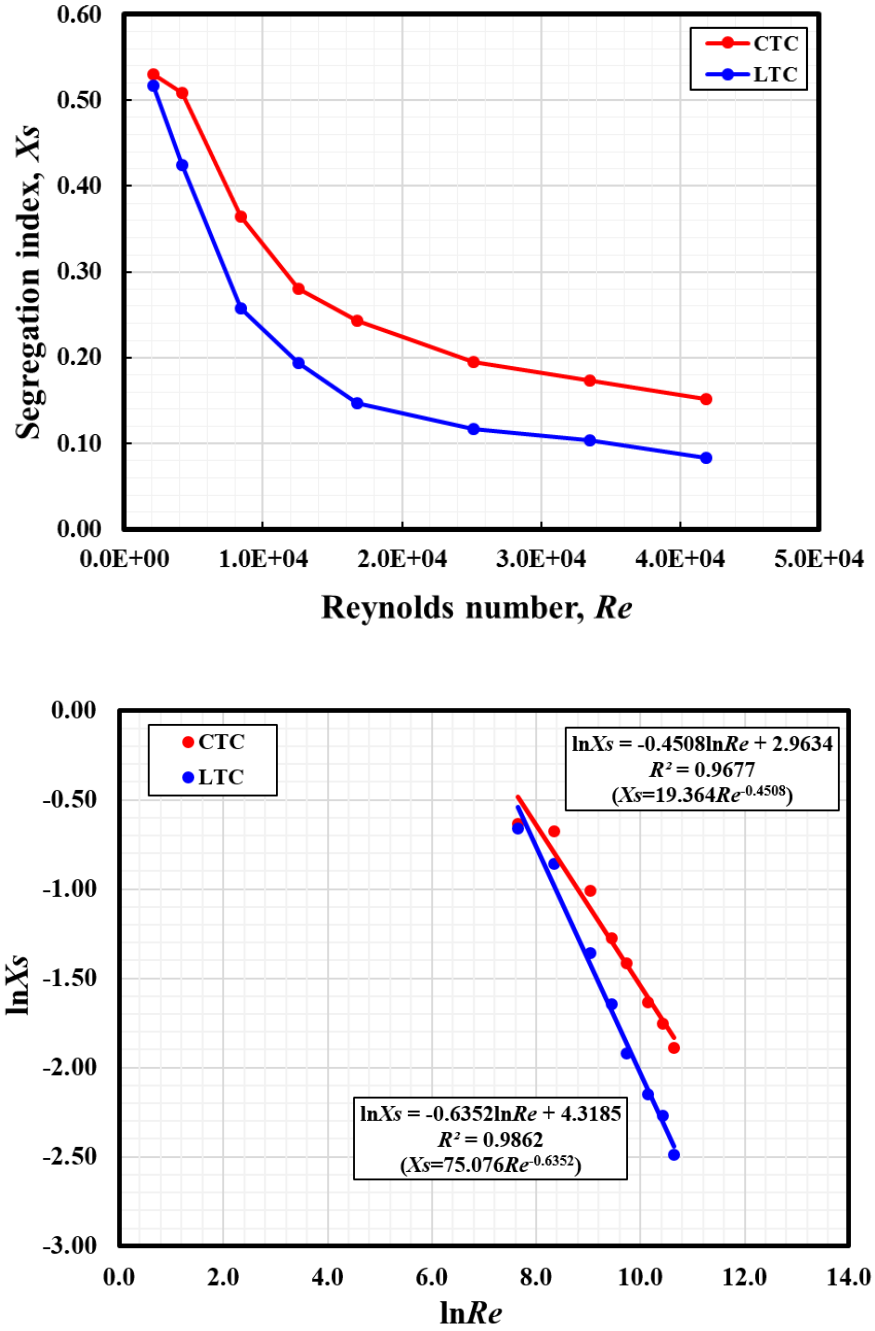


Figure 5. Effect of H^+ concentration on segregation index.



(a) (b)

Figure 6. (a) Effect of Reynolds number on segregation index; and (b) Segregation index as a function of Reynolds number

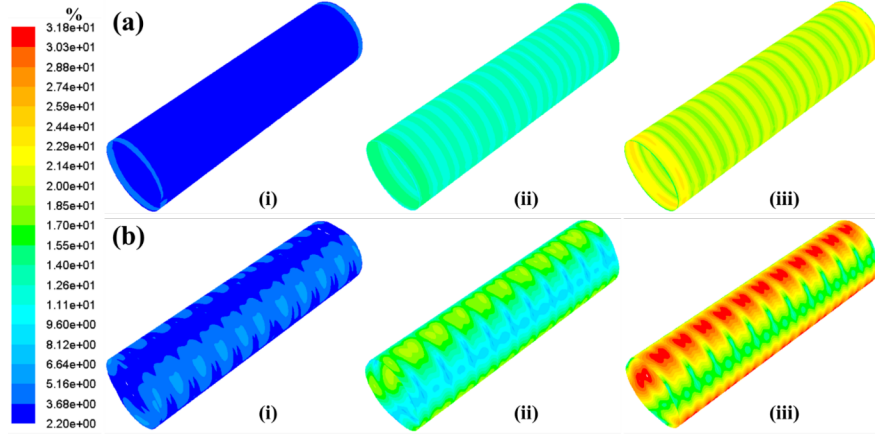


Figure 7. Distribution of the turbulent intensity on the surface of the inner cylinder: (a) CTC; and (b) LTC at different Reynolds number: (i): 4188; (ii) 25128; and (iii) 41880.

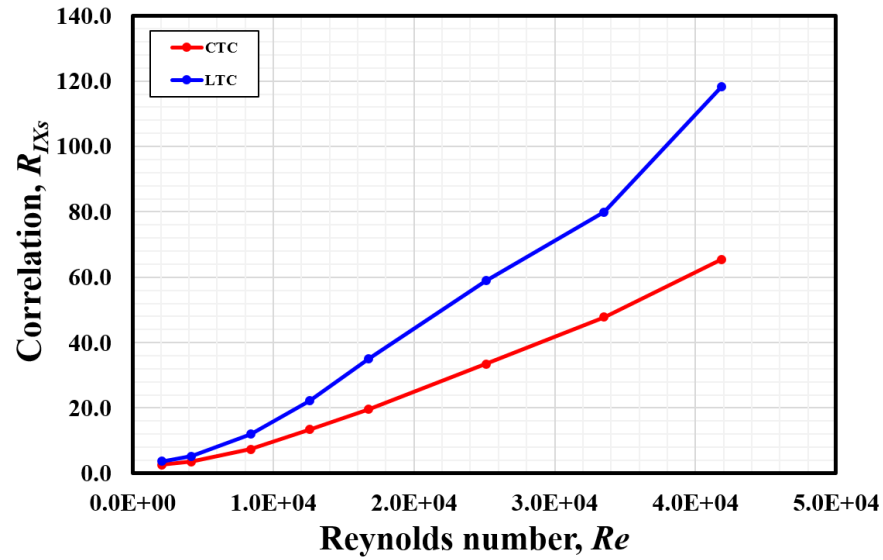


Figure 8. Correlation between the turbulent intensity and segregation index at different Reynolds numbers.

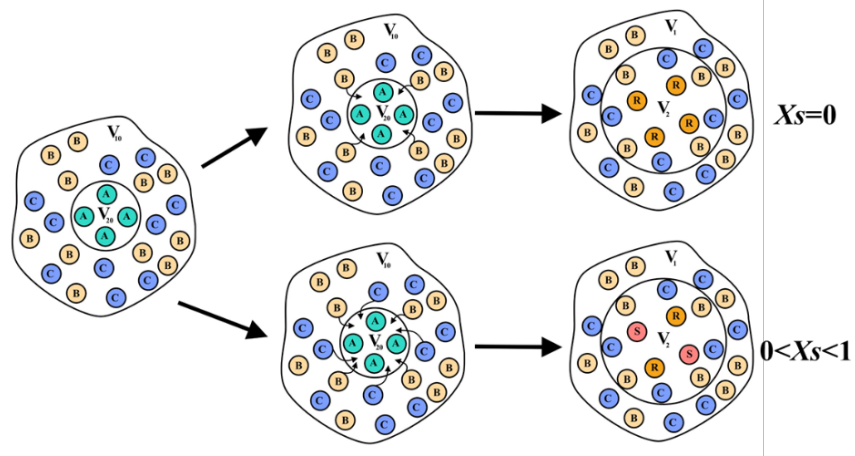


Figure 9. Principle of micromixing process based on the incorporation model.

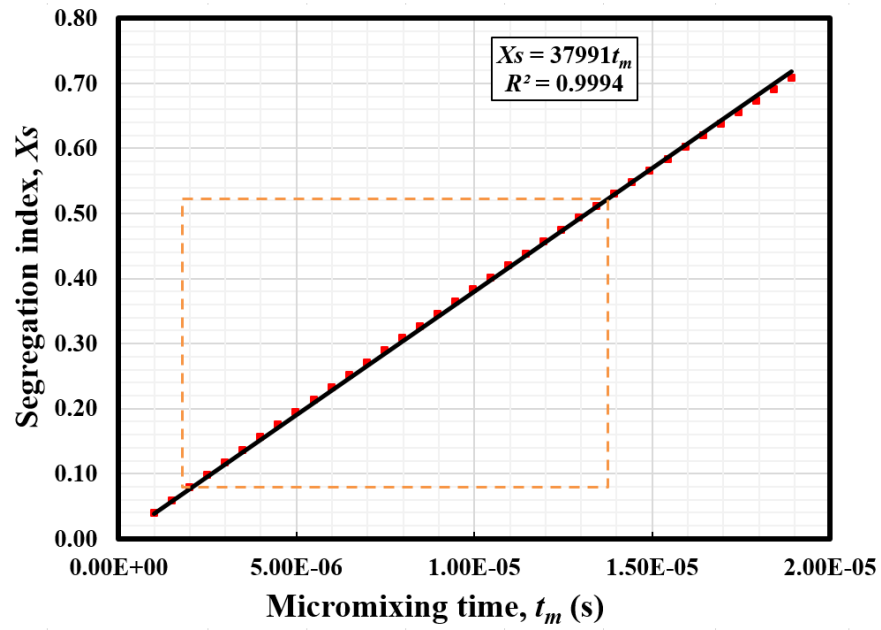


Figure 10. Predicted segregation index and micromixing time based on the incorporation model.

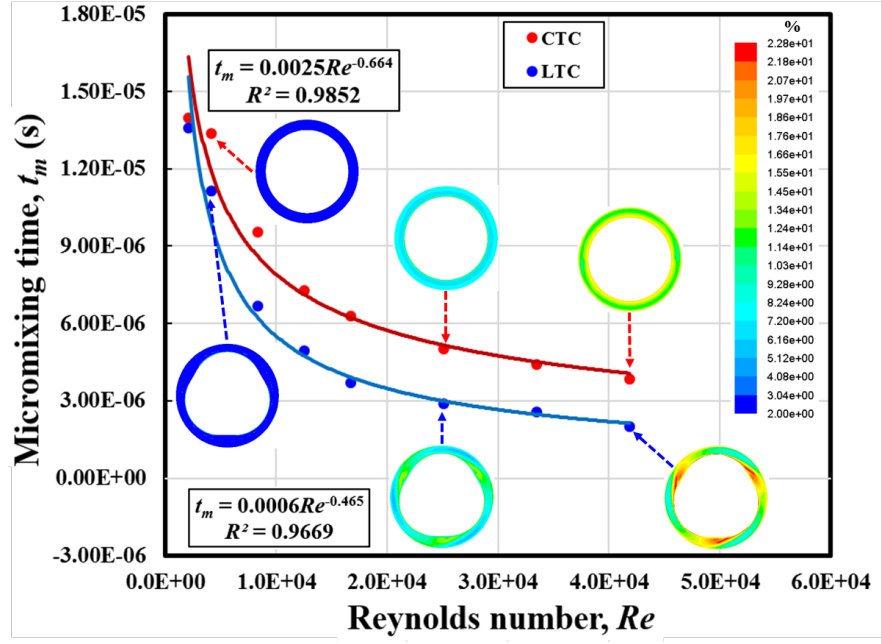


Figure 11. Micromixing time as a function of Reynolds number.